An overview of the ACE-2 clear sky column closure experiment (CLEARCOLUMN)

Philip B. Russell & Jost Heintzenberg

An overview of the ACE-2 clear sky column closure experiment (CLEARCOLUMN)

By PHILIP B. RUSSELL[1]* and JOST HEINTZENBERG[2,] [1]*NASA Ames Research Center, Moffett Field, CA 94035-1000 USA; [2]Institute for Tropospheric Research (IFT), 04318 Leipzig, Germany

ABSTRACT

As 1 of 6 focused ACE-2 activities, a clear sky column closure experiment (CLEARCOLUMN) took place in June/July 1997 at the southwest corner of Portugal, in the Canary Islands, and over the eastern Atlantic Ocean surrounding and linking those sites. Overdetermined sets of volumetric, vertical profile and columnar aerosol data were taken from the sea surface to ~ 5 km asl by samplers and sensors at land sites (20–3570 m asl), on a ship, and on 4 aircraft. In addition, 5 satellites measured upwelling radiances used to derive properties of the aerosol column. Measurements were made in a wide range of conditions and locations (e.g., the marine boundary layer with and without continental pollution, the free troposphere with and without African dust). Numerous tests of local and column closure, using unidisciplinary and multidisciplinary approaches, were conducted. This paper summarizes the methodological approach, the experiment sites and platforms, the types of measurements made on each, the types of analyses conducted, and selected key results, as a guide to the more complete results presented in other papers in this special issue and elsewhere. Example results include determinations of aerosol single scattering albedo by several techniques, measurements of hygroscopic effects on particle light scattering and size, and a wide range in the degree of agreement found in closure tests. In general, the smallest discrepancies were found in comparisons among (1) different techniques to measure an optical property of the ambient, unperturbed aerosol (e.g., optical depth, extinction, or backscatter by sunphotometer, lidar, and/or satellite) or (2) different techniques to measure an aerosol that had passed through a common sampling process (e.g., nephelometer and size spectrometer measurements with the same or similar inlets, humidities and temperatures). Typically, larger discrepancies were found between techniques that measure the ambient, unperturbed aerosol and those that must reconstruct the ambient aerosol by accounting for (a) processes that occur during sampling (e.g., aerodynamic selection, evaporation of water and other volatile material) or (b) calibrations that depend on aerosol characteristics (e.g., size-dependent density or refractive index). A primary reason for the discrepancies in such cases is the lack of validated hygroscopic growth models covering the necessary range of particle sizes and compositions. Other common reasons include (1) using analysis or retrieval techniques that assume aerosol properties (e.g., density, single scattering albedo, shape) that do not apply in all cases and (2) using surface measurements to estimate column properties. Taken together, the ACE-2 CLEARCOLUMN data set provides a large collection of new information on the properties of the aerosol over the northeast Atlantic Ocean. CLEARCOLUMN studies have also pointed to improved techniques for analyzing current and future data sets (including satellite data sets) which will provide a more accurate and comprehensive description of the Atlantic–European–African aerosol. Thus they set the stage for an improved regional quantification of radiative forcing by anthropogenic aerosols.

* Corresponding author.
e-mail: prussell@mail.arc.nasa.gov

1. Introduction

The clear sky column closure experiment (CLEARCOLUMN) is 1 of 6 focused activities conducted as part of the 2nd Aerosol Characterization Experiment (Raes et al., 2000; Verver et al., 2000). The purpose of CLEARCOLUMN is to evaluate the uncertainty in methods used to assess the direct radiative forcing of aerosols over the North Atlantic. The approach is to use over-determined sets of aerosol optical properties measured in columns and profiles and connected through radiation models. In each column, the experiment measured or derived the aerosol parameters needed to quantify the direct radiative forcing of the tropospheric aerosol. The satellites involved in this study can then be used to relate the direct radiative forcing derived in CLEARCOLUMN and in other columnar experiments to the larger North Atlantic region (Bergstrom and Russell, 1999). CLEAR-COLUMN addresses the 3rd ACE-2 scientific question (Raes et al., 2000):

> Can the measured physical and chemical properties of the aerosol in the vertical column be used to accurately predict the integrated direct effect of aerosols on radiative transfer?

CLEARCOLUMN used a 3-pronged closure approach to address this question.

(1) From extinction, scattering, and physico-chemical aerosol measurements at several ground elevations, on the ship, on airborne platforms, and in lidar beam profiles, unidisciplinary and multidisciplinary *local closure* can be tested at different altitudes in the boundary layer and free troposphere.

(2) Vertical integrals of the profile information can be compared to columnar extinction data derived from surface-based and air- and space-borne radiometers (supported by data on water-leaving radiances from ship- and airborne platforms) in order to test *column closure* of aerosol optical properties.

(3) Radiative fluxes from measurements can be compared to corresponding results derived by means of radiative transfer modeling from the aerosol and trace-gas measurements.

2. Methodological approach

CLEARCOLUMN took place in June/July, 1997, near Sagres, Portugal, in the Canary Islands, and over the eastern Atlantic Ocean surrounding and linking those sites. Fig. 1 shows a schematic overview of sites and platforms, and Table 1 lists coordinates of the land sites used in CLEARCOLUMN. Table 2 lists measurements made at or on each CLEARCOLUMN platform.

The central site near Sagres was S-50 (Table 2a) where the most powerful lidar was stationed together with sun and sky radiometry, stellar radiometry, boundary layer meteorology and a radiosonde. The lidar scanned in elevation angle, from near horizontal over the ocean west of Sagres, through the vertical, and towards the slopes of Mt. Fóia (900m asl) where radiometric, meteorological and aerosol characterisation instrumentation was set up at two altitudes (900 and 500 m asl).

The mountain top site near Sagres (S-900, Table 2c) was most representative for the upper part of the regional boundary layer and free troposphere aerosol. Thus S-900 was the second

Table 1. *Coordinates of land sites used in CLEARCOLUMN*

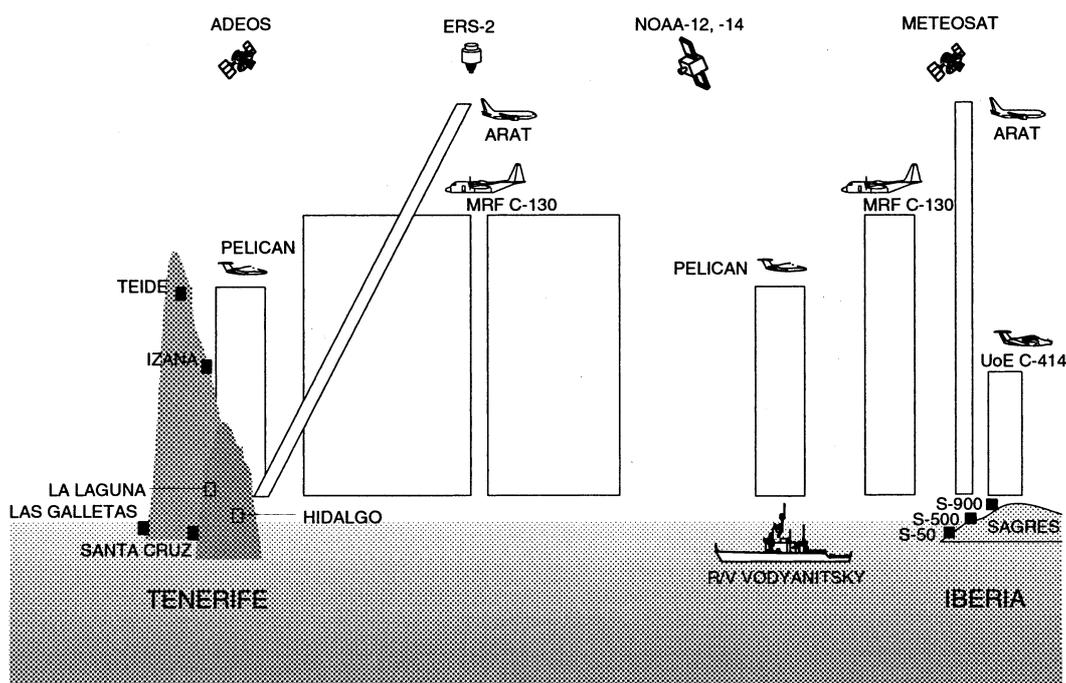| Site	Acronym	Longitude	Latitude	Altitude (m asl)
Sagres-50	S50	8° 57′W	36° 59′N	50
Sagres-500	S500	8° 37′W	36° 19′N	500
Sagres-900	S900	8° 37′W	36° 19′N	900
Las Galletas	LG	16° 39′W	28° 0′N	25
San Cristobal de La Laguna	SCLL	16° 29′W	28° 29′N	600
Santa Cruz	SC	16° 14′W	28° 29′N	10
Punta del Hidalgo	PDH	16° 19′W	28° 34′N	42
Izaña	IZO	16° 30′W	28° 18′N	2360
Teide	TEI	16° 36′W	28° 16′N	3570

Fig. 1. Schematic overview of CLEARCOLUMN sites and platforms.

Sagres site with an intensive aerosol characterisation. A ship (R/V Vodyanitskiy, Table 2d) on suitable trajectories leading to or from the Sagres area was equipped with another lidar, a tracking sunphotometer, and a suite of aerosol characterisation instruments. The boundary layer aerosol optical measurements at the Sagres surface sites were connected through flight missions by a C-414 aircraft (cf. Table 2j) carrying a spectral radiometer. Within and above the boundary layer, two research aircraft (MRF C-130 and the French ARAT, Tables 2k, 2l) flew vertical profiles and horizontal transects over the Sagres area to connect the sites and to extend the aerosol characterisation well into the free troposphere.

On the island of Tenerife in the Canaries, the Punta del Hidalgo lighthouse site (Table 2e) and the Izaña mountain ridge observatory (Table 2g) had extensive suites of instrumentation to characterize aerosol chemical, physical, and optical properties in the marine boundary layer and free troposphere, respectively. Included were sun/sky radiometers at both sites and an elevation-scanning MicroPulse lidar (MPL) at Izaña. Two additional sites near sea level, Santa Cruz de Tenerife

and Las Galletas (Table 2f), operated radiometers; Las Galletas also had a scanning MPL. Sun and sky radiometers were also operated at San Cristobal de La Laguna (Table 2f). The site near the summit of Teide (Table 2h) operated shadow-band and sun/sky radiometers.

The Pelican aircraft (Table 2i) measured aerosol chemical, physical, and optical properties, plus radiative fluxes and meteorological parameters, from sea level to ~ 4 km asl. Radiances measured by sensors on five satellites (ADEOS, ERS-2, NOAA-12, NOAA-14, METEOSAT; Fig. 1 and Table 2m) were used to derive aerosol and other properties.

2.1. Methodology for evaluation

For the evaluation of the field data a clearly-defined evaluation scheme was formulated that reached beyond the presentation of quality controlled data to a central ACE-2 data base and beyond the goals of CLEARCOLUMN proper towards the overall objectives of ACE-2 aiming at the regional quantification of radiative forcing in

Table 2a. *Measurements made at the Sagres 50 site*

Property measured	Principal investigator	Institution
Aerosol chemical		
aerosol ionic mass, size segregated	C. Neusüß	Institute for Tropospheric Research
aerosol carbon mass, size segregated	C. Neusüß	Institute for Tropospheric Research
Aerosol physical and optical		
aerosol size distributions (DMPS & APS)	A. Wiedensohler	Institute for Tropospheric Research
aerosol backscatter and extinction profiles (lidar)	F. Wagner	Institute for Tropospheric Research
RH controlled light scattering	M. Rood	University of Illinois
aerosol optical depth at 13 wavelengths (IR-RAD)	V. Vitale	FISBAT Bologna
Ångström turbidity parameter (IR-RAD)	V. Vitale	FISBAT Bologna
aerosol optical depth at 12 wavelengths (UVISIR-1)	V. Vitale	FISBAT Bologna
Ångström turbidity parameter (UVISIR-1)	V. Vitale	FISBAT Bologna
aerosol optical depth at 10 wavelengths (sun and star photometry)	W. Von Hoyningen-Huene	University of Leipzig
Ångström turbidity (sun and star photometry)	W. Von Hoyningen-Huene	University of Leipzig
normalized sky brightness	W. Von Hoyningen-Huene	University of Leipzig
Meteorological and others		
vertical wind profiles (SODAR)	M. L. Bugalho	University of Evora
surface meteorology	M. L. Bugalho	University of Evora
radio soundings (Sagres)	F. Wagner	Institute for Tropospheric Research
radio soundings (S. Teotonio)	M. L. Bugalho	University of Evora
radiative fluxes (downwelling global and diffuse)	A. M. Silva,	University of Evora
	W. Von Hoyningen-Huene	University of Leipzig

Table 2b. *Measurements made at the Sagres-500 site*

Property measured	Principal investigator	Institution
Aerosol optical		
aerosol optical depth at 7 wavelengths (UVISIR-2)	V. Vitale	FISBAT Bologna
Ångström turbidity parameter (UVISIR-2)	V. Vitale	FISBAT Bologna
aerosol optical depth at 10 wavelengths (sun photometry)	W. Von Hoyningen-Huene	University of Leipzig
Ångström turbidity (sun photometry)	W. Von Hoyningen-Huene	University of Leipzig
normalized sky brightness	W. Von Hoyningen-Huene	University of Leipzig

the polluted marine atmosphere. Fig. 2 shows a flow chart of this methodology.

After primary quality control and derivation of physical quantities from the individual measured parameters the results were segregated into air mass and aerosol types. A variety of closure tests (Quinn et al., 1996) were then conducted, yielding multiparameter evaluations of the degree of consistency or inconsistency between experimental and modeling approaches. A number of 'Golden Days' were defined, on which to focus the initial data evaluation. For Sagres data, these days are listed in Table 3. Two time periods were selected for detailed analyses: 1997-06-20 ± 2 days as clean marine reference days and 1997-07-20 ± 2 days as the period with highest continental aerosol burden. Golden days for the Tenerife area were 21 June and 8, 10, and 17 July. For the ship they

Table 2c. *Measurements made at the Sagres 900 site*

Property measured	Principal investigator	Institution
Aerosol chemical		
aerosol ionic mass (PM-10 sampler)	C. Neusüß	Institute for Tropospheric Research
Aerosol physical and optical		
aerosol size distribution (DMPS)	A. Wiedensohler	Institute for Tropospheric Research
aerosol absorption coefficient	A. M. Silva, M. L. Bugalho	University of Evora
aerosol optical depth at 12 wavelengths (UVISIR-1)	V. Vitale	FISBAT Bologna
Ångström turbidity parameter (UVISIR-1)	V. Vitale	FISBAT Bologna
aerosol optical depth at 14 wavelengths (sun photometry)	M. J. Costa, A. M. Silva	University of Evora
aerosol scattering and back scattering coefficients at 3 wavelengths	M. Bugalho, A. M. Silva	University of Evora
aerosol optical depth at 10 wavelengths (sun photometry)	W. Von Hoyningen-Huene	University of Leipzig
Ångström turbidity (sun photometry)	W. Von Hoyningen-Huene	University of Leipzig
normalized sky brightness	W. Von Hoyningen-Huene	University of Leipzig
Meteorological and others		
48-h back trajectories (800, 925, 1000 hPa) and meteorological analysis (925, 1000 hPa)	M. Bugalho, A. M. Silva	University of Evora
radiative fluxes (downwelling global and diffuse)	A. M. Silva, W. Von Hoyningen-Huene	University of Evora University of Leipzig

were 24, 27, and 30 June and 6, 10, and 22 July. 10 July included measurements by the Pelican near the ship to the northeast of the Canary Islands.

3. Results

3.1. Surface-based volumetric data

Complete aerosol size distributions have been derived at Sagres 50 (Neusüß et al., 2000) and submicrometer size distributions at Mt. Fóia (Sagres-900) (Henning et al., 1998). Grand average distributions for clean marine and polluted periods clearly show that pollution aerosols were observed at both sites and that the coastal site always was under marine influence with a significant coarse particle component. Simultaneous co-located measurements of aerosol light scattering, hemispheric backscattering, and chemical composition permitted tests of closure with the size distribution measurements. Also on the research vessel concurrent physical, chemical and optical data were collected for optical closure tests (Bates et al.,

2000; Quinn et al., 2000). Trajectory analyses show that both continental and marine flows were sampled by the ship, and different trajectories produced systematic differences in a variety of chemical and optical properties (see below).

Hygroscopic growth properties of the aerosol are crucial parameters which are required to connect volumetric aerosol data measured at reduced relative humidity to optical aerosol properties derived at ambient relative humidities. Thus the ACE-2 program included such growth measurements at the land-based sites (Swietlicki et al., 2000; Carrico et al., 2000), onboard the research vessel (Livingston et al., 2000; Quinn et al., 2000), and on the Pelican aircraft (Gassó et al., 2000).

For the interpretation of both chemical and optical data the carbonaceous aerosol component (both organic and inorganic) is of particular importance. Measurements of aerosol light absorption are also critical, both for direct use in determining aerosol optical properties such as single scattering albedo, and for estimation of equivalent black carbon amounts using empirical conversion factors. Consequently, most of the

Table 2d. *Measurements made aboard the R/V Vodyanitskiy**

Property measured	Principal investigator	Institution
Atmospheric chemical		
aerosol ionic mass, coarse and fine fraction	P. Quinn	PMEL NOAA
aerosol ionic mass, size segregated (Berner impactor)	P. Quinn	PMEL NOAA
aerosol OC and EC, coarse and fine fraction	T. Bates	PMEL NOAA
Aerosol physical and optical		
particle number, $D_p > 15$ nm	T. Bates	PMEL NOAA
aerosol size distribution (Twin DMA + APS)	T. Bates	PMEL NOAA
hygroscopic growth factors for $D_p = 50$–250 nm	B. Busch	Institute for Tropospheric Research
aerosol total mass, coarse and fine	P. Quinn	PMEL NOAA
aerosol scattering, backscattering, and backscattered fraction at 3 wavelengths with $D_p < 1$ μm	P. Quinn	PMEL NOAA
aerosol scattering, backscattering coefficients at 3 wavelengths with $D_p < 10$ μm	P. Quinn	PMEL NOAA
aerosol absorption, scattering, and single scattering albedo at 550 nm.	P. Quinn	PMEL NOAA
aerosol optical depth, 4 wavelengths	R. Frouin	University of California at San Diego
aerosol optical depth, 4 wavelengths (handheld sunphotometers)	P. Quinn	PMEL NOAA
aerosol optical depth at 5 wavelengths, water vapor column (AATS-6)	P. Russell	NASA Ames
lidar backscatter at 1064 nm	V. Freudenthaler	University of München
Meteorology and others		
radiosoundings	J. Johnson	PMEL NOAA
water-leaving radiance	R. Frouin	University of California at San Diego

*cf. Johnson et al. (2000) for complete list.

CLEARCOLUMN platforms and sites and also long term ACE-2 aerosol measurements included measurements of aerosol carbon and/or light absorption, concurrent with other chemical, physical, and optical measurements (Quinn et al., 2000; Novakov et al., 2000; Neusüß et al., 2000; Putaud et al., 2000).

For Sagres-50 data Neusüß et al. (2000) report a 3-way comparison of size-resolved mass concentrations derived from (1) gravimetric analysis of impactor samples (collected and analyzed at 60% RH), (2) chemical analysis of the impactor samples, and (3) number-size distributions measured concurrently by Twin Differential Mobility Analyser (TDMPS) and Aerodynamic Particle Counter (APS) (both at RH < 10%). Chemical results are reported for Cl^-, NO_3^-, SO_4^{2-}, NH^{4+}, Na^+, Mg^{2+}, K^+, Ca^{2+}, volatile and nonvolatile carbon, and water. For submicrometer particles,

water uptake was calculated using hygroscopic growth factors measured for size-segregated particles in the diameter range 35–250 nm; for super-micrometer particles seasalt growth factors from Tang et al. (1997) were used. Overall, Neusüß et al. find that masses derived by each method agree within the combined uncertainties, which they estimate to be about $\pm 20\%$ for each method when masses are integrated over geometric diameters $D_p < 3$ μm. Results are expressed as slopes of linear regression fits obtained when comparing pairs of methods for 15 cases ranging from clean to polluted (total masses 5 to 40 μg m^{-3}). For example, they find that, on average, masses for $D_p < 3$ μm derived from TDMPS/APS number-size distributions were 23% larger than corresponding masses determined gravimetrically from impactor samples. Analogously, chemical masses for $D_p < 3$ μm were on average 2% larger than

Table 2e. *Measurements made at Punta del Hidalgo*

Property measured	Principal investigator	Institution
Atmospheric chemistry		
aerosol ionic mass, coarse and fine fraction	J. P. Putaud	Joint Research Centre, Ispra
aerosol carbon mass, fine fraction	J. P. Putaud	Joint Research Centre, Ispra
aerosol ionic mass, size segregated (MOUDI impactor)	A. Allen	University of Birmingham
aerosol ionic mass, size segregated (Sierra impactor)	H. Sievering	University of Colorado
aerosol ionic mass, coarse and fine fraction	N. Hewitt	University of Lancaster
elemental aerosol concentration ratios of H, C, N, O, K, Ca, V and Br to S ($D_p < 1$ μm)	E. Swietlicki	University of Lund
Aerosol physical and optical		
aerosol size distributions and integrated number, surface area and volume (DMA)	R. Van Dingenen	Joint Research Centre, Ispra
aerosol size distribution $D_p > 0.4$ μm (TSI-APS)	E. Swietlicki	University of Lund
ratio of CCN (0.2 and 0.5%) to CN at specific dry sizes	P. Aalto	University of Helsinki
hygroscopic growth factors for $D_p = 0.035$–0.44 μm	E. Swietlicki	University of Lund
aerosol absorption coefficient—equivalent black carbon concentration	R. Van Dingenen	Joint Research Centre, Ispra
aerosol optical depth spectra and sky radiance (AERONET Cimel)	B. Holben	NASA Goddard

Table 2f. *Measurements made at Santa Cruz de Tenerife, San Cristobal de La Laguna, and Las Galletas*

Property measured	Principal investigator	Institution
Aerosol optical measurements at Santa Cruz De Tenerife		
aerosol optical depth (AOD) from sun photometery	J. P. Diaz	University of La Laguna
aerosol optical depth spectra and polarized sky radiance (LOA Cimel)	T. Elias	Laboratoire d'optique Atmospherique, Villeneuve dÁscq, France
Aerosol optical measurements at San Cristobal de La Laguna		
aerosol optical depth spectra and polarized sky radiance (LOA RefPol, Cimel)	T. Elias	Laboratoire d'optique Atmospherique, Villeneuve dÁscq, France
Aerosol optical measurements At Las Galletas		
aerosol backscatter and extinction (Micro-Pulse lidar)	J. Reagan	University of Arizona
aerosol optical depth from sun photometry at 10 wavelengths	J. Reagan	University of Arizona

the corresponding gravimetric masses. Results are also given for size classes corresponding to 4 or 5 impactor stages. Relative mass differences and uncertainties were found to depend on size class, but were independent of the degree of pollution.

Also for Sagres-50 data Philippin et al. (1998; personal communication) performed tests of local optical closure for the dry submicrometer aerosol by comparing measured scattering and backscattering coefficients at wavelength 550 nm with values calculated from measured size distributions and chemical compositions. For scattering coefficients they found best agreement when they modeled the aerosol as an internal mixture of sulfate and nonvolatile carbon with size-resolved mass fractions from three impactor stages.

From samples taken aboard R/V Vodyanitskiy (Table 2d) at 10 m asl, Novakov et al. (2000) found concentrations of aerosol organic carbon (OC) that averaged 0.89 μg m^{-3} for submicro-

Table 2g. *Measurements made at Izaña**

Property measured	Principal investigator	Institution
Atmospheric chemical		
SO_2 (LC)	J. P. Putaud	Joint Research Centre, Ispra
elemental aerosol concentration of H, C, N, O, S, K, Ca, V and Br ($D_p < 1 \mu m$)	E. Swietlicki	University of Lund
single particle elemental composition and size	R. Van Grieken	University of Antwerp
aerosol ionic mass, coarse and fine fraction	J. P. Putaud	Joint Research Centre, Ispra
aerosol carbon mass, fine fraction	J. P. Putaud	Joint Research Centre, Ispra
Aerosol physical and optical		
aerosol sub-μm size distribution and integrated number, surface area and volume (DMA)	R. Van Dingenen	Joint Research Centre, Ispra
hygroscopic growth factors for $D_p = 10$ and 50 nm	J. Mäkelä	University of Helsinki
volatility shrink factor for $D_p = 10$ and 50 nm	J. Mäkelä	University of Helsinki
aerosol backscatter and extinction profiles (micropulse lidar)	J. Welton (H. Gordon)	University of Miami
aerosol optical depth spectra and sky radiance (AERONET Cimel)	B. Holben	NASA Goddard
aerosol optical depth spectra and polarized sky radiance (LOA Cimel, RefPol)	T. Elias	Laboratoire d'optique Atmospherique, Villeneuve dÁscq, France

*Partial list.

Table 2h. *Measurements made at Teide*

Property measured	Principal investigator	Institution
Aerosol physical and optical		
aerosol optical depth spectra (YES shadow-band radiometer)	M. Andreae	Max Planck Institute for chemistry, Mainz
aerosol optical depth spectra and sky radiance (AERONET Cimel)	M. Andreae	Max Planck Institute for chemistry, Mainz

meter aerosols during polluted conditions. This average is similar to the averages for OC measured at Sagres (0.61 μg m^{-3}) and Punta del Hidalgo (0.64 μg m^{-3}) during polluted conditions (Putaud et al., 2000). By combining measured submicron nonseasalt sulfate (nss SO_4^{2-}) and black carbon (BC), Novakov et al. (2000) found nss SO_4^{2-}/BC ratios that averaged 12 over the ACE-2 Vodyanitskiy cruise, very similar to the average SO_4^{2-}/BC ratio of 11 measured off the eastern US coast in aircraft samples at altitudes between 100 and 3000 m asl during TARFOX (Novakov et al., 1997; Hegg et al., 1997). (The distinction between nss SO_4^{2-} and total SO_4^{2-} was unimportant for

the TARFOX samples, because the TARFOX inorganic analysis yielded sulfate as the only anion present above trace levels, and mass budget closure was obtained within 10% by using only sulfate and carbonaceous measurements compared to total masses from filters.)

In contrast, ratios of sulfate to total carbon (TC) differed significantly between ACE-2 Vodyanitskiy samples and TARFOX samples. Vodyanitskiy nss SO_4^{2-}/TC ratios averaged 5.3 ± 2.9 for submicron aerosol samples and 2.9 ± 1.3 for submicron plus supermicron samples. TARFOX SO_4^{2-}/TC ratios were negatively correlated with altitude, averaging 1.6 ± 0.7 at the lowest

Table 2i. *Measurements made aboard the Pelican aircraft*

Property measured	Principal investigator	Institution
Aerosol chemical		
aerosol ionic mass, carbon, and trace metals in fine fraction $< 2.5\ \mu m$	L. Russell	Princeton University
Aerosol and cloud physical and optical		
size distributions (DMA)	D. Collins (R. Flagan/J. Seinfeld)	California Institute of Technology
size distributions (PCASP, FSSP)	H. Jonsson	California Institute of Technology
CCN spectra (0.1% supersaturation)	P. Chuang (R. Flagan/J. Seinfeld)	California Institute of Technology
aerosol scattering and absorption	K. Noone	Stockholm University
aerosol scattering, wet and dry	S. Gassó	University of Washington
aerosol optical depth at 13 wavelengths and water vapor column (AATS-14)	P. Russell	NASA Ames Research Center
Meteorological and other		
position, meteorology	H. Jonsson	CIRPAS
radiative fluxes	H. Jonsson	CIRPAS
T, RH, pressure	S. Gassó	University of Washington

Table 2j. *Measurements made aboard C-414 aircraft*

Property measured	Principal investigator	Institution
Aerosol optical		
Spectral upwelling radiances at 230 m and 520 m height (0.45–0.52; 0.52–0.60; 0.60–0.63; 0.63–0.69; 0.70–0.75; 0.91–1.05 μm) by spectralradiometer	M. Silva	University of Evora

sampling altitudes (100– 300 m asl), 1.2 over all TARFOX filter sampling altitudes (100–3000 m), and 0.6 ± 0.6 above 2500 m. Since the TARFOX aerosol intake system collected particles with $D_p \leqslant 5\ \mu m$, it is most appropriate to compare the Vodyanitskiy submicron plus supermicron SO_4^{2-}/TC ratio of 2.9 ± 1.3 to the TARFOX ratio of 1.6 ± 0.7 at 100–300 m. Even with this selected comparison, the TARFOX SO_4^{2-}/TC ratio is significantly less than the Vodyanitskiy ratio, indicating larger aerosol organic carbon fractions in TARFOX than in the Vodyanitskiy samples. It is interesting to note that at Izaña (2360 m asl, Table 2g), Putaud et al. (2000) measured submicron nss SO_4^{2-}/TC of 0.71 in background conditions and 0.36 in flows from North America. These values suggest that both increasing altitude and a North American origin tend to reduce nss

SO_4^{2-}/TC, reflecting larger aerosol organic carbon fractions.

By combining shipboard measurements of aerosol light scattering and absorption (for $D_{aero} < 10\ \mu m$, at RH 55% and wavelength 550 nm), Quinn et al. (2000) obtained single scattering albedo values that had mean and standard deviation 0.95 ± 0.03 in continental flows (range 0.81 to 0.99) and 0.98 ± 0.01 in marine flows (range 0.93 to 0.99). Their technique for measuring absorption, which used a Particle Soot Absorption Photometer, included an empirically-derived correction factor to account for the small (1 to 1.5%) positive artifact caused by instrumental interpretation of scattering as absorption. Quinn et al. (2000) also report a significant relationship between air mass origin and the wavelength dependence of aerosol light scattering, $\sigma_{sp}(\lambda)$.

Table 2k. *Measurements aboard the C-130 aircraft**

Property measured	Principal investigator	Institution
Atmospheric chemical		
aerosol ionic mass, coarse and fine fraction	A. Andreae	Max Planck Institute for chemistry, Mainz
Aerosol and cloud physical and optical		
particles, $D_p > 3$ nm (TSI 3025)	D. Johnson	Meteorological Research Flight, Farnborough
Particles, $D_p > 100$ nm (PCASP)	D. Johnson	Meteorological Research Flight, Farnborough
particles, $D_p > 500$ nm (FSSP)	D. Johnson	Meteorological Research Flight, Farnborough
heated/ambient aerosol size distributions (VACC/SMPS)	C. O'Dowd	U. Sunderland
aerosol scattering and absorption	D. Johnson	Meteorological Research Flight, Farnborough
CCN spectra	D. Johnson	Meteorological Research Flight, Farnborough
Meteorological and others		
broad band radiometers	D. Johnson	Meteorological Research Flight, Farnborough

*See LAGRANGIAN overview paper (Johnson et al., 2000) for complete list.

Table 2l. *Measurements aboard the ARAT aircraft**

Property measured	Principal investigator	Institution
Aerosol and cloud physical and optical		
particles > 300 nm (PMS ASASP)	J. Pelon	Institut National des Sciences de l'Univers, Paris
aerosol extinction coefficient from airborne lidar LEANDRE	J. Pelon	Institut National des Sciences de l'Univers, Paris
Meteorology and others		
position, winds, thermodynamics, radiation, etc.	J. Pelon	Institut National des Sciences de l'Univers, Paris

*See CLOUDYCOLUMN overview paper (Brenguier et al., 2000) for complete list.

Specifically, the Ångström exponent ($a \equiv -d \ln \sigma_{sp}(\lambda)/d \ln \lambda$) between 550 and 700 nm for $D_{aero} < 10$ μm at 55% RH was 1.2 ± 0.3 in continental flows and 0.24 ± 0.26 in marine flows. This reflects the increased importance of scattering by submicrometer aerosols in continental flows. At Sagres-50 for RH 27% and $D_{aero} < 10$ μm, Carrico et al. (2000) found Ångström exponents of 1.48 ± 0.26 and 0.57 ± 0.34 during pollution outbreaks and "clean" periods, respectively.

Carrico et al. (2000) combined nephelometer measurements of aerosol light scattering and aethalometer derived light absorption estimates for particles with $D_{aero} < 10$ μm (RH < 30%) to obtain single scattering albedos ω (550 nm). Their best estimate of ω (550 nm) at RH 27% during pollution outbreaks at Sagres-50 is 0.94 with an uncertainty of 0.02. During "clean" periods the corresponding best estimate was 0.93 with the same uncertainty. Their measured effects of aerosol hygroscopic growth on light scattering increased ω (550 nm) by about 0.01, assuming light absorption is independent of RH. Given uncertainties in the aethalometer measurement (Heintzenberg

Table 2m. *Measurements made on satellites*

Property measured	Principal investigator	Institution
METEOSAT images 6-h, VIS, IR and WV (GIF)	M. Van Liedekerke	Joint Research Centre, Ispra
METEOSAT full data; VIS, IR and WV channels	M. Van Liedekerke	Joint Research Centre, Ispra
aerosol optical depth and ratio Ch1/Ch2 (NOAA14–AVHRR, GIF)	F. Exposito	University of La Laguna, Tenerife
aerosol optical depth, ERS-2/ATSR	G. de Leeuw	TNO-FEL, the Hague, Netherlands
aerosol optical depth at 630, 860 nm (NOAA-12, -14 AVHRR; METEOSAT imager)	P. Durkee	Naval Postgraduate School, Monterey, CA
aerosol optical depth, ADEOS/POLDER	D. Tanré	Laboratoire d'optique Atmospherique, Villeneuve dÁscq, France
aerosol optical depth, ADEOS/OCTS	T. Nakajima	University of Tokyo

et al., 1997) and the range of air masses and RH at Sagres-50, they estimate the range of ω (550 nm) there as 0.91 to 0.97.

3.2. Profile and column data

At Sagres 50 and onboard the research vessel multiwavelength lidar profiles were taken throughout the ACE-2 experiment, spanning conditions from clean marine aerosol in a shallow boundary layer through European pollution filling most of the first 3 km altitude range. From the Sagres-50 profiles height-dependent in-situ aerosol size distributions were inverted (Wagner et al., 1998). The lidar profiles also yielded boundary layer heights and limits of elevated aerosol layers which compared very well with concurrent local radiosonde temperature profiles.

Welton et al. (2000) present micropulse lidar measurements of upslope aerosols and African dust layers over Izaña on Tenerife (Table 2g). They use an iterative algorithm that incorporates simultaneous sunphotometer optical depth measurements to derive height-independent backscatter-to-extinction ratios at the single lidar wavelength (523 nm) and thereby obtain vertical profiles of aerosol extinction and optical depth. Comparisons between an independent optical depth measurement on the Teide summit (3570 m asl, Table 2h, Formenti et al., 2000) and the lidar value at that altitude yielded agreement to within 0.01, in both upslope and dust-layer conditions (optical depth

range 0.003 to 0.075). Comparison to an airborne sunphotometer profile (Schmid et al., 2000) within the dust layer yielded differences of ± 0.02 or less at all altitudes (~ 2500–3800 m asl), over which optical depth decreased from 0.22 to 0.05.

Powell et al. (2000) report measurements of marine boundary layer and desert dust aerosols made with the micropulse lidar at Las Galletas on the southern tip of Tenerife (Table 2f). They used the slant-sensing technique of measuring profiles at several zenith angles, which, together with an assumption of horizontal and temporal homogeneity during the scanning period, yields layer optical depths and backscatter-to-extinction ratios. This information was then employed when the lidar was vertically pointing to obtain the temporal evolution of backscatter, extinction, and optical depth profiles. The attenuation of horizontal lidar profiles was also used to determine the extinction coefficient at the lidar altitude. Comparisons to airborne sunphotometer measurements of layer optical depth (Schmid et al., 2000) produced differences of ± 0.01 for dust and boundary-layer aerosol optical depths (which were 0.24 and 0.05, respectively, at the lidar wavelength of 530 nm).

Flamant et al. (2000) report airborne lidar measurements and closure studies for a European pollution outbreak sampled by the ARAT aircraft (Table 2l). The lidar mapped vertical profiles of the pollution plume and the marine boundary layer aerosol as the plume was carried from the
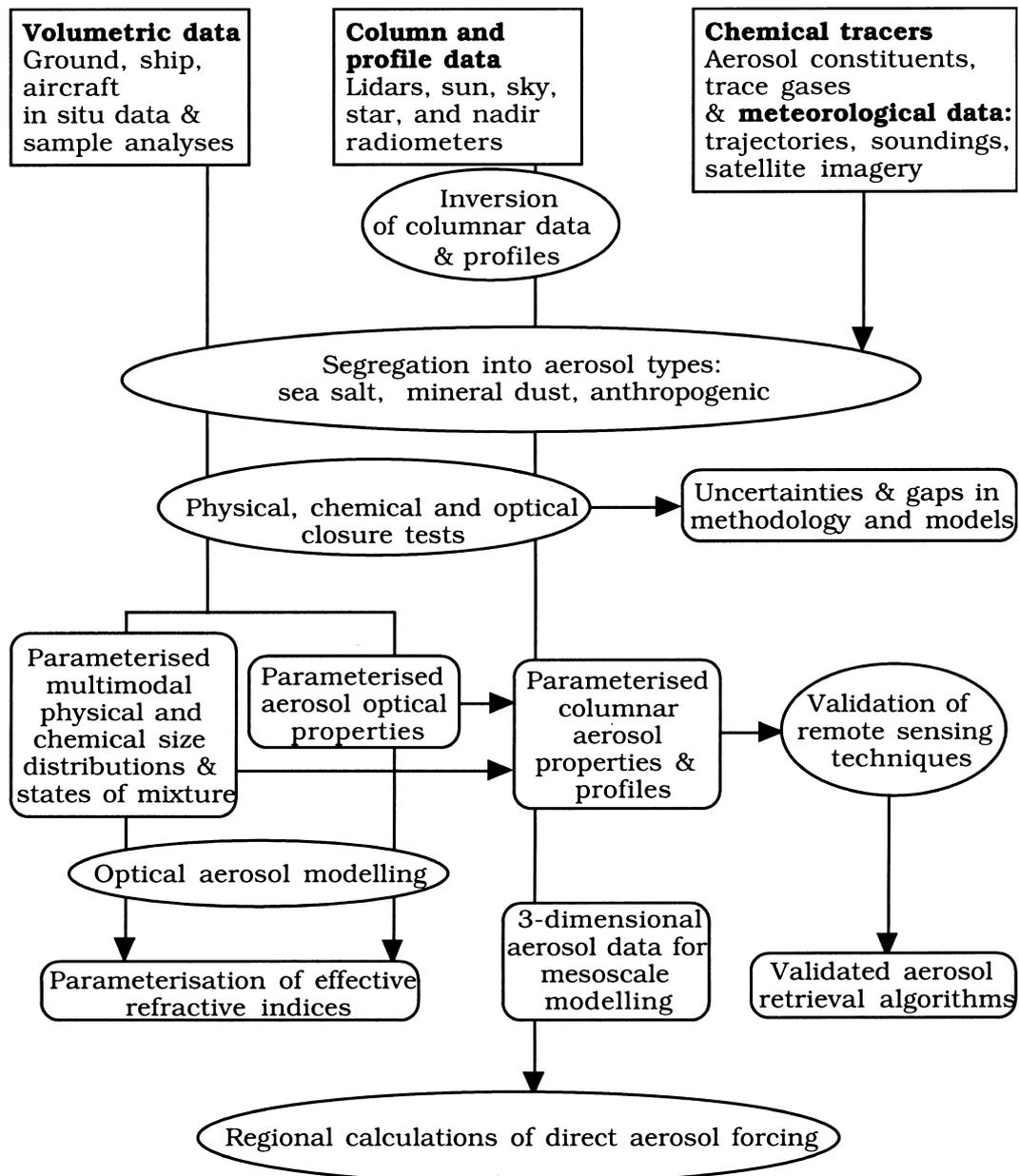
Volumetric data
Ground, ship,
aircraft
in situ data &
sample analyses

**Column and
profile data**
Lidars, sun, sky,
star, and nadir
radiometers

Chemical tracers
Aerosol constituents,
trace gases
& **meteorological data:**
trajectories, soundings,
satellite imagery

Inversion
of columnar data
& profiles

Segregation into aerosol types:
sea salt, mineral dust, anthropogenic

Physical, chemical and optical
closure tests

Uncertainties & gaps in
methodology and models

Parameterised
multimodal
physical and
chemical size
distributions &
states of mixture

Parameterised
aerosol optical
properties

Parameterised
columnar
aerosol
properties &
profiles

Validation of
remote sensing
techniques

Optical aerosol modelling

3-dimensional
aerosol data for
mesoscale
modelling

Parameterisation of effective
refractive indices

Validated aerosol
retrieval algorithms

Regional calculations of direct aerosol forcing

Fig. 2. Flow chart of the evaluation methodology of CLEARCOLUMN. Squares mark input data. Ovals stand for processing steps and rounded rectangles indicate deliverables.

coast of Portugal near Sagres over the ship and beyond over the Atlantic Ocean. Particle extinction profiles were derived from the lidar data using an extinction coefficient at a reference height and parameterized model profiles of backscatter-to-extinction ratio (BER). The reference extinction was obtained using free-tropospheric nephelometer measurements on the ARAT; model BER

Table 3. *Periods initially chosen for CLEARCOLUMN data evaluation in the Sagres area. Julian day is defined here such that noon on 1 February equals Julian day 31.5*

Chosen day	Start Julian day	End Julian day	Start date	Time GMT	End date	Time GMT
1	166.8	167.8	970616	19:12	970617	19:12
2	170.8	171.4	970620	19:12	970622	9:36
3	172	172.25	970622	0:00	970622	6:00
4	174	174.3	970624	0:00	970624	7:12
5	177.8	179.8	970627	19:12	970629	19:12
6	180.5	181.2	970630	12:00	970701	4:48
7	182.5	184	970702	12:00	970704	0:00
8	188	189.3	970807	0:00	970709	7:12
9	189.8	190.3	970907	19:12	970710	7:12
10	190.3	190.9	971007	7:12	970710	21:36
11	193.5	194.8	970713	12:00	970714	19:12
12	197.5	198.5	970717	12:00	970718	12:00
13	201.5	202.3	970721	12:00	970722	7:12
14	202.3	202.75	970722	7:12	970722	18:00
15	203	203.65	970723	0:00	970723	15:36

profiles were obtained using size distribution spectra measured on the ship and on the ARAT. lidar-derived extinction profiles at 0.55 μm differed from nephelometer-measured scattering profiles by ~0.03 km^{-1} or less. Values of aerosol optical depth (AOD) derived from the lidar ranged from 0.055 to 0.10. When compared to ship sunphotometer measurements, differences were 0.02 or less, within the combined lidar and sunphotometer uncertainties. In contrast, AODs derived from METEOSAT radiances exceeded the lidar values by 0.01 to 0.08, with the largest differences in the area where the pollution plume contributed most to column optical depth. Flamant et al. suggest that the difference may be caused by large uncertainties associated with the Meteosat sensitivity for small AODs or by the presence of thin scattered clouds.

At all Sagres sites multiwavelength sun and sky photometry yielded aerosol optical thickness spectra, sky brightness distributions and phase functions (Bugalho et al., 1998; Vitale et al., 2000; Von Hoyningen-Huene, 1998). The Sagres photometer measurements were also used to derive columnar amounts of precipitable water (Tomasi et al., 2000). At Sagres-50 a star photometer for the first time provided night time aerosol optical thickness spectra which were complementary and consistent with the daytime data yielding diurnal in situ aerosol optical variations over the whole experiment (Von Hoyningen-Huene et al., 1998; personal

communication). These data show, for example, that wind shifts associated with the diurnal cycle in land-sea air exchange were accompanied by systematic changes in both aerosol optical thickness and its wavelength dependence. In particular, when wind shifted from WNW to ENE during evening and night hours, the aerosol optical thickness δ at wavelength 1 μm decreased and the wavelength exponent ($\alpha \equiv -\mathrm{d}\ln \delta(\lambda)/\mathrm{d}\ln \lambda$) increased.

Von Hoyningen-Huene et al. (1998; personal communication) also combined measurements of optical depth wavelength dependence, sky brightness angular dependence, and radiative fluxes at Sagres-900 (Table 2c) to obtain best-fit values for the single scattering albedo ω of the ambient (hydrated) column aerosol, averaged over all solar wavelengths. In this way they obtained $\omega = 0.98 \pm 0.03$ for maritime-influenced conditions (8 cases) and 0.90 ± 0.04 for polluted continental conditions (6 cases). (All cases were without African dust.) They also found that, for maritime-influenced cases at both Sagres-50 and Sagres-900, the aerosol phase functions they derived from sky brightness measurements could be fitted better with a scattering theory for non-spherical particles than with the Mie theory for homogeneous spheres. Measured scattering phase functions for maritime-influenced cases with low relative humidity (RH < 78%) differed more from Mie phase functions than did measured maritime-influenced

phase functions for high-humidity periods (RH > 78%). They attributed these results to asphericity of seasalt particles, especially in low-humidity conditions. In continental air masses Mie-theory phase functions fitted the measured phase functions well.

Tenerife sun and sky photometer measurements from within the boundary layer and in the free troposphere are reported by Smirnov et al. (1998), Formenti et al. (2000), and Elias et al. (2000). They provide results for optical depth, wavelength dependence, and column aerosol phase functions, documenting the systematic changes that occurred on the several occasions when African dust was carried over Tenerife (e.g., increasing optical depth, decreasing wavelength dependence, decreased polarized phase function at 60° scattering angle).

Shipboard sunphotometer measurements of aerosol optical depth (AOD) spectra and column water vapor (CWV) are reported by Livingston et al. (2000). Comparisons between CWV measured by sunphotometer and by radiosonde yielded good agreement, with an rms difference of 0.09 g cm^{-2} in 7 samples having a CWV range of 1.6 to 3.2 g cm^{-2}. AODs inferred from shipboard aerosol lidar backscatter measurements during one day were consistent with those measured by the shipboard sunphotometer, but the uncertainties associated with deriving optical depth from the shipboard lidar data were large ($\sim$factor 2) because of the need to assume an extinction-to-backscatter ratio that differed for maritime and continental-influenced aerosols. Livingston et al. (2000) also performed column closure tests between AODs measured by sunphotometer and computed by combining shipboard particle size distribution measurements with models of hygroscopic growth and radiosonde humidity profiles (using the assumption that dry particle size distribution and composition were independent of height in the boundary layer). These closure tests often produced big discrepancies, in large part because of their great sensitivity to models of hygroscopic growth, which vary considerably and have not been validated over the necessary range of particle size/composition distributions. The wavelength dependence of shipboard sunphotometer AODs was compared with the corresponding dependence of aerosol extinction calculated from shipboard measurements of aerosol size distribution and of total scattering measured by a shipboard integrating nephelometer. Results of these comparisons were highly variable, illustrating again the great difficulty of deriving column values from point measurements.

Profile data from the Pelican aircraft (Table 2i) have been used in a variety of ways to study both boundary-layer and free-tropospheric aerosols. For example, Collins et al. (2000) combine vertical profiles of Pelican-measured particle number-versus-size spectra with size-resolved chemical compositions to derive scattering, hemispheric backscattering, and extinction coefficient profiles and compare them to the measurements of Öström and Noone (2000), Gassó et al. (2000) and Schmid et al. (2000). The size-resolved chemical compositions used in each case are based on boundary-layer and free-tropospheric measurements made at Punta del Hidalgo and Izaña (Tables 2e, 2g; Putaud et al., 2000) and are also consistent with the size-integrated compositions measured on the Pelican aircraft and reported by Schmeling et al. (2000). Collins et al. use the hygroscopic properties of the aerosol constituents to derive size-resolved particle densities and refractive indices and thereby account for the sampling processes that affect each particle prior to detection (e.g., inlet aerodynamic size selection, evaporation by ram-air and sheath-air heating) as well as the size calibration of optical particle counters. This permits reconstructing the ambient aerosol that existed before its distortion by sampling processes (as is needed for comparison to, e.g., sunphotometer measurements—see below), as well as the aerosol within dried and humidified nephelometers at specified humidities (Gassó et al., 2000; Öström and Noone, 2000).

Schmeling et al. (2000) report aerosol chemical composition measurements from samples collected aboard the Pelican. They derive spectra of ambient aerosol refractive index for each sample by combining their aerosol species results with the Howell and Huebert (1998) parameterization for water vapor uptake and with published species refractive index spectra. They note, however, that their imaginary refractive index results are subject to underestimation, because sampling constraints resulted in detection limits for elemental carbon that were between 1% and 3% of total sample mass, and in fact all samples had carbon below the detection limit.

Gassó et al. (2000) report measurements of

hygroscopic effects on aerosol light scattering measured by a passive humidigraph on the Pelican. The passive humidigraph uses two nephelometers, one designed to operate below ambient RH, and the other above. Particle scattering coefficients σ_{sp} at wavelength 530 nm from the two nephelometers are used to solve for the exponent γ in the equation

$$\sigma_{sp}(\text{RH}) = k(1 - \text{RH}[\%]/100\%)^{-\gamma}. \qquad (1)$$

The value of γ is then used to estimate σ_{sp} at the ambient RH, and also to estimate $\sigma_{sp}(80\%)/\sigma_{sp}(30\%)$ $(= [0.7/0.2]^{\gamma})$. Gassó et al. note that since eq. (1) does not account for deliquescence and hysteresis effects, their approach is more applicable to aerosols where these effects are expected to be small, or to dust aerosols, where hygroscopicity is itself expected to be small. They present results for a vertical profile of γ, obtained on a case when Pelican descended through an African dust layer at 3800–2600 m ASL and into the polluted marine boundary layer (1000–50 m asl); values of γ in the dust and polluted marine layers were ~ 0.15 and 0.55, respectively. Over all ACE-2 Pelican flights they obtained γ values that had mean and standard deviation 0.23 ± 0.05 for dust (7 samples), 0.57 ± 0.06 for polluted marine aerosols (37 samples), and 0.69 ± 0.06 for clean marine aerosols (21 samples). Corresponding values of $\sigma_{sp}(80\%)/\sigma_{sp}(30\%)$ are 1.33 ± 0.07, 2.04 ± 0.16, and 2.37 ± 0.19. These results are in qualitative agreement with previous results reported by Hegg et al. (1996), Covert et al. (1972), Fitzgerald et al. (1982), and Kotchenruther et al. (1999). However, they significantly exceed the results obtained at Sagres-50 by Carrico et al. (2000), who performed increasing and decreasing controlled RH scans with two nephelometers in series.

Schmid et al. (2000) compare airborne sunphotometer-measured optical depth profiles to vertical integrals of the Collins et al. results. Their sunphotometer optical depth profiles are also differentiated vertically to yield extinction profiles, which are compared to the profiles mentioned above. For the two cases in which an elevated African dust layer was sampled, AOD values from sunphotometer and in situ size distributions agreed to within 7.5% for wavelengths $\lambda = 380$ to 1060 nm. However, at $\lambda = 1558$ nm, values from in situ size distributions exceeded sunphotometer values by $\sim 20\%$. Schmid et al. note that the difference might be caused by an incorrect assumed refractive index at 1558 nm, but that refractive index measurements covering the full 380–1558 nm range are lacking. In the marine boundary layer both Schmid et al. and Collins et al. note a tendency for extinction and optical depth values from in situ size distributions to be somewhat less than sunphotometer values (e.g., by 10%, 25%, and 15%, and on 8, 10, and 17 July, respectively). Although they both note that these differences are within the combined uncertainties, Schmid et al. point out that the sign of the difference (in situ < sunphotometer) is the same as in several previous studies, and they suggest possible reasons for this commonality (see "Summary and conclusions", below).

Schmid et al. also compare their sunphotometer optical depths and extinctions to those obtained from the nephelometer and absorption photometer measurements of Gassó et al. (2000) and Öström and Noone (2000) on the same aircraft. Optical depth differences ΔAOD ranged from $+15\%$ to -44%, significantly exceeding ΔAOD in the size distribution/sunphotometer comparisons. Schmid et al. attribute the larger differences to the fact that the nephelometer and absorption photometer sampled the aerosol through a cyclone with aerodynamic cutoff diameter 2.5 μm, whereas the size distribution measurements did not. Although inlet cyclone correction factors were applied to the nephelometer and absorption photometer values, the factors were relatively large (e.g., 1.17–1.47 in the MBL and 2.8–3.2 in the dust), and their uncertainties could have accounted for the AOD differences obtained.

Schmid et al. also report comparisons between size distributions measured in situ and retrieved from the wavelength dependence of sunphotometer optical depths and extinctions. They note that agreement was better in the MBL than in the elevated dust layer, with differences in the dust layer possibly attributable to the lack of refractive index information covering the full 380–1558 nm range noted above.

The Pelican measurements also demonstrated for the first time agreement between vertical profiles of column water vapor (CWV) derived from sunphotometer-measured transmission and obtained by integrating profiles from radiosonde and airborne hygrometer. The agreement was

typically within ± 0.15 g cm^{-2} in profiles from the surface to 3.8 km with CWV values ranging from 0.2 to 1.7 g cm^{-2}. The airborne sunphotometer CWV profiles were also differentiated vertically to yield profiles of water vapor density, producing values that agreed typically to within ± 1 g cm^{-3} with radiosonde and airborne hygrometer values that ranged from 0.1 to 17 g cm^{-3} (Schmid et al., 2000; Livingston et al., 2000).

Values of aerosol single scattering albedo ω determined from scattering and absorption measurements made aboard Pelican (Öström and Noone, 2000) varied considerably. Flight-leg means and standard deviations in the boundary layer at altitudes 980 to 30 m ranged from 0.75 ± 0.43 to 0.96 ± 0.19 for the dry aerosol; corresponding upper limits for the ambient aerosol at 90% RH ranged from 0.89 to 0.99. Flight-leg means within African dust layers at altitudes 3250 to 3885 m varied from 0.73 ± 0.12 to 0.91 ± 0.11 (Öström and Noone, 2000).

3.3. Satellite studies and comparisons

(Durkee et al., 2000) present a regional view of ACE-2 aerosol properties derived from advanced very high resolution radiometer (AVHRR) radiance measurements on the NOAA-14 satellite and compare results to those obtained in ACE-1 and TARFOX. They also compare AVHRR optical depths at 630 and 860 nm with values measured in ACE-2 by a variety of sunphotometers on land, ship, and the Pelican aircraft (Schmid et al., 2000; Livingston et al., 2000). For the 23 cases that met coincidence criteria (described in detail by Durkee et al.), the correlation coefficient between AVHRR and sunphotometer optical depths was 0.93 for 630 nm wavelength and 0.92 for 860 nm wavelength. The standard error of estimate was 0.025 for 630 nm wavelength and 0.023 for 860 nm wavelength. Included in the comparison were three cases where African dust was present. In these cases, AVHRR optical depths systematically underestimated sunphotometer optical depths, by amounts ranging from 0.01 to 0.08 (with optical depths ranging from ~ 0.3 to 0.4). As Durkee et al. note, agreement for the dust cases would be improved by changing the nonabsorbing aerosol optical model used in the AVHRR retrievals to an absorbing one; dust aerosol shape effects on the scattering phase function should also be con-

sidered (Mishchenko et al., 1997). Because there were only 3 cases of African dust in the intercomparison, they had little effect on the overall correlation and rms difference reported above.

Using the AVHRR optical depths, Durkee et al. point out some interesting features of the spatial patterns and frequency distributions of ACE-2 aerosol optical depths in comparison to those from ACE-1 and TARFOX. For example, they note the rather wide range of ACE-2 aerosol optical depths, from very clean to polluted. This produced, for example, an ACE-2 mode optical depth at 630 nm of 0.095, actually less than the ACE-1 mode of 0.115. The ACE-2 mean aerosol optical depth was 0.162, falling between the ACE-1 and TARFOX values of 0.130 and 0.353, respectively. The ACE-2 standard deviation was 0.109, larger than the ACE-2 mode (reflecting the broad, skewed ACE-2 distribution) and nearly 4 times the ACE-1 standard deviation. Values quoted in this paragraph are for wavelength 630 nm; similar contrasts with ACE-1 and TARFOX were observed at 860 nm.

Von Hoyningen-Huene et al. (1999; personal communication) present results of a study comparing ground-based aerosol optical thickness (AOT) measurements at Sagres-50, Sagres-500 (Monchique), and Sagres-900 (Mt. Foia) with retrievals from the Ocean Color and Temperature Sensor (OCTS) on the ADEOS satellite (Table 2m). They first perform radiative transfer calculations to predict top-of-atmosphere (TOA) radiances measured in OCTS channels 1–8 (center wavelengths 0.412–0.865 μm). These calculations use aerosol optical depths and scattering phase functions derived from ground-based sun and sky radiometer measurements as described by Von Hoyningen-Huene et al. (1998; personal communication) and summarized above. When they use the phase functions that best fit their sky brightness measurements, they find root-mean-square differences (RMSD) of $<5\%$ between calculated and OCTS-measured radiances for OCTS channels 4–8 (0.520–0.865 μm), and somewhat larger RMSD for channels 1–3. As noted above, these best-fit phase functions are obtained using a scattering theory for nonspherical particles. In contrast, using spherical-particle phase functions (for the marine aerosol cases they consider) produces significantly different relationships between TOA radiance and AOT. They report that using these

spherical-particle relationships in AOT retrievals from TOA radiances would yield AOTs too large by a factor of ~ 2 in the near-infrared channels (6–8). By using look-up tables of TOA radiance vs. AOT based on their nonspherical particle phase functions they retrieve AOT spectra over the ocean for OCTS channels 4–8 on three days (14, 16, and 18 June 1997). Results are presented as images of the Ångström fitting parameters α and β defined by $AOT(\lambda) = \beta(\lambda[\mu m])^{-\alpha}$, where β is AOT (1 μm). Comparisons of α and β values measured by sunphotometer at Sagres-50, Sagres-500, and Sagres-900 with corresponding OCTS-retrieved values at nearby pixels over the ocean yielded differences of typically ± 0.2 in α and ± 0.03 in β.

4. Summary and conclusions

CLEARCOLUMN provided a detailed data set of clear sky aerosol properties at many surface sites of the ACE-2 area reaching from Tenerife to South West Portugal and including ship borne measurements. The near-sea-level data were complemented by measurements at mountain sites at different altitudes up to 3570 m asl. Aircraft measurements connected the surface based data and extended the data set in the vertical. The aerosol characteristics are available for different air masses ranging from clean marine air comparable to the ACE-1 environment to polluted air masses from the European continent. In the southernmost part of the working area, Saharan dust outbreaks were encountered on several occasions. The combined data set includes the 3-dimensional variability of physical and chemical aerosol characteristics as a function of particle size and aerosol type, thus providing the basic information for regional assessments of aerosol effects.

While many of the aerosol characteristics were derived at reduced relative humidities, large data sets on particle growth and change of optical parameters with humidity were obtained at several sites and on the Pelican aircraft. With that information the data set can in principle be converted to ambient thermodynamic conditions. However, the fact that particle growth measurements could usually be made only for diameters up to 250 nm, coupled with some unexplained disagreements between different measures of

hygroscopic effects on light scattering, calls for further study.

With the volumetric aerosol data several closure tests were made. At Sagres-50 a 3-way comparison of size-resolved mass concentrations from gravimetric, chemical, and number distributions (Neusüß et al., 2000) produced agreement within state of the art experimental uncertainties (estimated at $\pm 20\%$ for each method for mass integrated over all $D_p < 3$ μm).

State of the art columnar optical aerosol measurements were made at the CLEARCOLUMN sites. Beyond the usual spectral and angular parameters, polarization characteristics were measured on Tenerife extending the range of aerosol information and connecting the ground based optical data to satellite borne polarisation measurements with the POLDER instrument (Elias et al., 2000). At several surface and airborne positions aerosol parameters were retrieved with different methodologies from remotely sensed optical measurements with inversion and retrieval algorithms, thus deriving ambient size distributions and intensive particle properties such as their refractive index as a function of aerosol types (Von Hoyningen-Huene et al., 1998; personal communication; Wagner et al., 1998; Schmid et al., 2000). In a few experiments these derived aerosol properties were compared to volumetric aerosol measurements to test the quality of the retrieval. Among the difficulties in these comparisons were the technical limitations in measuring supermicrometer aerosol properties from an aircraft.

CLEARCOLUMN determined aerosol single scattering albedos ω by a variety of techniques in a wide range of aerosol conditions. Values determined from dry (27% RH) aerosol light scattering and absorption measurements at the Sagres-50 ground site in Portugal yielded ω (550 nm) = 0.94 ± 0.02 and 0.93 ± 0.02 for pollution outbreaks and "clean" periods, respectively (Carrico et al., 2000). Considering measurement uncertainties and the range of air masses and RH at Sagres-50, they estimate the range of ambient ω (550 nm) there as 0.91 to 0.97. Shipboard measurements of aerosol scattering and absorption at 55% RH yielded a somewhat larger difference in ω (550 nm) between cases of continental flow and marine flow, with values of 0.95 ± 0.03 and 0.98 ± 0.01, respectively (Quinn et al., 2000). Also, ω derived from best fits of calculated to measured solar radiative fluxes

(Von Hoyningen-Huene et al., 1998; personal communication) yielded values for the hydrated, ambient column aerosol of 0.90 ± 0.04 for polluted continental cases and 0.98 ± 0.03 for maritime-influenced cases (both without African dust).

The differences in single scattering albedo obtained by different techniques (0.90 ± 0.04 to 0.95 ± 0.03 for nominally polluted cases) may not be statistically significant given the quoted uncertainties and variabilities. Nevertheless, aerosol single scattering albedos of 0.90 and 0.95 can yield significantly different aerosol climatic effects over realistic surfaces (Haywood and Shine, 1995; Hansen et al., 1997; Russell et al., 1997). Thus it is important to determine whether the differences in ω reflect different aerosols or different measurement and analysis techniques. This points to a need for increased emphasis in future experiments on (a) simultaneous measurements of the same air mass by different techniques, and (b) standardized methods of deriving ω from, e.g., in situ scattering and absorption measurements (Anderson and Ogren, 1998; Bond et al., 1999), so that measurements made at different times and places can be compared directly.

ACE-2 tests of column closure produced a wide range of results. Tests that produced relatively small discrepancies included comparisons of: (1) African dust extinction and optical depth spectra ($\lambda = 380$ to 1060 nm) determined by airborne sunphotometer to those computed from measured size distributions using multicomponent size-resolved compositions based on ACE-2 measurements (Collins et al., 2000; Schmid et al., 2000), (2) aerosol optical depths for the humid marine boundary layer ($RH > 80\%$) as measured by sunphotometer to those retrieved from radiances measured by the satellite sensors AVHRR and OCTS (Durkee et al., 2000; Schmid et al., 2000; Livingston et al., 2000; Von Hoyningen-Huene et al., 1999; personal communication), and (3) African dust aerosol optical depth profiles measured by airborne sunphotometer and retrieved from lidar backscatter (Schmid et al., 2000). In tests of type (1) and (2) closure degraded for (1) African dust extinction and optical depth at $\lambda = 1558$ nm, owing possibly to refractive index errors at that wavelength, (2a) African dust optical depths at 630 and especially 860 nm, possibly caused by particle shapes and complex refractive indices not accounted for in AVHRR retrieval algorithms and

(2b) Relatively dry ($RH < 78\%$) marine boundary layer optical depths, attributed to particle asphericity not accounted for in OCTS retrieval algorithms.

In the marine boundary layer, optical depths or extinctions from airborne in situ measurements (particle size spectrometer, nephelometer, absorption photometer) were typically less than those from the airborne sunphotometer. Although differences between AODs from in situ size distributions and from sunphotometer were judged to be within the combined uncertainties, those uncertainties were significant (often $\sim 30\%$ or larger) and arose from many sources (the most important of which were, in most cases, uncertainties in sizing by mobility and optical analyzers, in aerosol mixing state (internal vs. external), in heating within the optical sizer, in the hygroscopicity of organics, and spatiotemporal variations of optical depth on the moving path between sunphotometer and sun). Differences between AODs from the nephelometer/absorption photometer combination and from the sunphotometer were larger still, probably because of large uncertainties in inlet cyclone correction factors. Nevertheless, as pointed out by Collins et al. (2000), the degree of agreement that was obtained in the aircraft vertical profiles is significant, because of the variety of instruments on board, each of which was sensitive to different aspects of the sampled aerosol. Agreement among this variety of measures limits the degree to which potential multiple errors in the size distribution and related analyses could simply offset one another, as might be the case if comparisons were limited to a single measurement at a single wavelength.

It is noteworthy that in the great majority of the ACE-2 Pelican comparisons, the sign of the AOD difference ($\Delta AOD = AOD_{\text{in situ}} - AOD_{\text{sunphotometer}}$) is negative, as was obtained in several previous studies (Clarke et al., 1996; Hegg et al., 1997; Remer et al., 1997; Hartley et al., 2000; Kato et al., a comparison of the aerosol optical thickness derived from ground-based and airborne measurements, submitted to *Journal of Geophysical Research*, 1999). Although reasons for these differences are currently speculative, some phenomena reported in the literature might provide at least partial explanations. These phenomena include (a) loss of semivolatile material (e.g., organics) in direct sampling (Eatough et al.,

1996), (b) gas absorption that might be present but is not accounted for in the sunphotometer analyses (Halthore et al., 1998), and/or (c) aerosol hygroscopic changes that can be greater than in the models used (Saxena et al., 1995).

Attempts to demonstrate closure between boundary layer optical depth spectra from sunphotometer and from shipboard dry particle size distributions grown using radiosonde humidity profiles often yielded large discrepancies (Livingston et al., 2000). A primary reason is the lack of validated hygroscopic growth models covering the necessary range of particle sizes and compositions. In general ACE-2 results point to unresolved differences between the hygroscopic changes in particle size and light scattering described by various measurements and models. Uncertainties in single scattering albedo also result in part from lack of knowledge of the effects of changing humidity on aerosol light absorption, another area that requires further investigation.

Taken together, the ACE-2 CLEARCOLUMN data set provides a large collection of new information on the properties of the aerosol over the northeast Atlantic Ocean. CLEARCOLUMN studies have also pointed to improved techniques for analyzing current and future data sets (including satellite data sets) that will provide a more accurate and comprehensive description of the Atlantic–European–African aerosol. Several ongoing studies to harmonize the underlying aerosol models used by remote retrieval algorithms with the corresponding measured aerosol properties will help in this regard. When these ongoing improvements and validations are complete, the combined volumetric and columnar data sets will provide the information for a regional quantification of radiative forcing by anthropogenic aerosols.

5. Acknowledgements

REFERENCES

Anderson, T. L. and Ogren, J. A. 1998. Determining aerosol radiative properties using the TSI 3563 integrating nephelometer. *Aer. Sci. Tech.* **29**, 57–69.

Bates, T., Quinn, P., Covert, D. S., Coffman, D. J. and Johnson, D. 2000. Aerosol properties and controlling processes in the lower marine boundary layer: a comparison of ACE-1 and ACE-2. *Tellus* **52B**, 258–272.

Bergstrom, R. W. and Russell, P. B. 1999. Estimation of aerosol radiative effects over the mid-latitude North Atlantic region from satellite and in situ measurements. *Geophys. Res. Lett.* **26**, 1731–1734.

Bond, T. C., Anderson, T. L. and Campbell, D. 1999. Calibration and intercomparison of filter-based measurements of visible light absorption by aerosols. *Aer. Sci. Tech.* **30**, 582–600.

Brenguier, J.-L. et al. 2000. An overview of the ACE-2 CLOUDYCOLUMN closure experiment. *Tellus* **52B**, 815–827.

Bugalho, M. L., Silva, A. M. and Von Hoyningen-Huene, W. 1998. Evaluation of spectral aerosol properties from sun-photometry and nephelometer measurements during ACE 2 CLEARCOLUMN. *J. Aerosol Sci.* **29**, S263–S264.

Carrico, C. M., Rood, M. J., Ogren, J. A., Neusüß, C., Wiedensohler, A. and Heintzenberg, J. 2000. Aerosol light scattering properties measured at Sagres, Portugal, during ACE-2. *Tellus* **52B**, 694–715.

Clarke, A. D., Porter, J. N., Valero, F. P. J. and Pilewskie, P. 1966. Vertical profiles, aerosol microphysics, and optical column closure during the Atlantic stratocumulus transition experiment: measured and modeled column optical properties. *J. Geophys. Res.* **101**, 4443–4453.

Collins, D. R., Jonsson, H. H., Seinfeld, J. H., Flagan, R. C., Gassó, S., Hegg, D., Russell, P. B., Livingston, J. M., Schmid, B., Öström, E., Noone, K. J. and Russell, L. M. 2000. In situ aerosol size distributions and clear column radiative closure during ACE-2. *Tellus* **52B**, 498–525.

Covert, D. S., Charlson, R. J. and Ahlquist, N. C. 1972.

A study of the relationship of chemical composition and humidity to light scattering by aerosols. *J. App. Met.* **11**, 968–976.

Durkee, P. A., Nielsen, K. E., Russell, P. B., Schmid, B., Livingston, J. M., Collins, D., Flagan, R. C., Seinfeld, H. H., Noone, K. J., Öström, E., Gassó, S., Hegg, D., Bates, T. S., Quinn, P. K. and Russell, L. M. 2000. Regional aerosol properties from satellite observation: ACE-1, TARFOX and ACE-2 results. *Tellus* **52B**, 484–497.

Eatough, D. J., Eatough, D. A. and Lewis, E. A. 1995. Fine particulate chemical composition and extinction apportionment at Canyonlands National Park using organic particulate material concentrations obtained with a multi-system, multichannel diffusion denuder sampler. *J. Geophys. Res.* **101**, 19515.

Elias, T., Devaux, C., Goloub, P., Tanré, D. and Herman, M. 2000. Polarising properties of the aerosols in the north-eastern tropical Atlantic Ocean, with emphasis on the ACE-2 period, *Tellus* **52B**, 620–635.

Fitzgerald, J. W. and Hoppel, W. A. 1982. The size and scattering coefficient of urban aerosol particles at Washington, DC as a function of relative humidity., *J. Atmos. Sci.* **39**, 1838–1852.

Flamant, C., Pelon, J., Chazette, P., Trouillet, V., Bruneau, D., Quinn, P., Frouin, R., Bruneau, D., Leon, J. F., Bates, T. Johnson, J. and Livingston, J. 2000. Airborne lidar measurements of aerosol spatial distribution and optical properties over the Atlantic Ocean during a European pollution outbreak of ACE-2. *Tellus* **52B**, 662–677.

Formenti, P., Andreae, M. O. and Lelieveld, J. 2000. Measurements of aerosol optical depth in the North Atlantic free troposphere: results from ACE-2. *Tellus* **52B**, 678–693.

Gassó, S., Hegg, D. A., Covert, D. S., Noone, K., Öström, E., Schmid, B., Russell, P. B., Livingston, J. M., Durkee, P. A. and Jonsson, H. 2000. Influence of humidity on the aerosol scattering coefficient and its effect on the upwelling radiance during ACE-2. *Tellus* **52B**, 546–567.

Halthore, R. N., Nemesure, S., Schwartz, S. E., Imre, D. G., Berk, A., Dutton, E. G. and Bergin, M. H. 1998. Models overestimate diffuse clear-sky surface irradiance: A case for excess atmospheric absorption. *Geophys. Res. Lett.* **25**, 3591–3594.

Hansen, J. M., Sato, M. and Ruedy, R. 1997. Radiative forcing and climate response. *J. Geophys. Res.* **102**, 6831–6864.

Hartley, W. S., Hobbs, P. V., Ross, J. L., Russell, P. B. and Livingston, J. M. 2000. Properties of aerosols aloft relevant to direct radiative forcing off the mid-Atlantic coast of the United States. *J. Geophys. Res.*, in press.

Haywood, J. M. and Shine, K. P. 1995. The effect of anthropogenic sulfate and soot aerosol on the clear sky planetary radiation budget. *Geophys. Res. Lett.* **22**, 603–606.

Hegg, D. A., Covert, D. S., Rood, M. J. and Hobbs, P. V. 1996. Measurement of the aerosol optical properties in marine air. *J. Geophys. Res.* **96**, 12883–12903.

Hegg, D. A., Livingston, J., Hobbs, P. V., Novakov, T. and Russell, P. B. 1997. Chemical apportionment of aerosol column optical depth off the mid-Atlantic coast of the United States, *J. Geophys. Res.* **102**, 25,293–25,303.

Heintzenberg, J., Charlson, R. J., Clarke, A. D., Liousse, C., Ramaswamy, V., Shine, K. P., Wendisch, M. and Helas, G. 1997. Measurements and modeling of aerosol single-scattering albedo: progress, problems, and prospects. *Beitr. Phy. Atmosph.* **70**, 249–263.

Henning, S., Weise, D., Birmili, W., Wiedensohler, A. and Covert, D. S. 1998. The particle size distribution and total number concentration for different air masses at the south-western edge of Europe. *J. Aerosol Sci.* **29**, S273–S274.

Howell, S. G. and Huebert, B. J. 1998. Determining marine and aerosol scattering characteristics at ambient humidity from size-resolved chemical composition. *J. Geophys. Res.* **103**, 1391–1404.

Johnson, D. et al. 2000. An overview of the Lagrangian experiments undertaken during the North Atlantic regional Aerosol Characterization Experiment (ACE-2). *Tellus* **52B**, 290–320.

Kotchenruther, R. A., Hobs, P. V. and Hegg, D. A. 1999. Humidification factors for atmospheric aerosol off the mid-Atlantic coast of United States. *J. Geophys. Res.* **104**, 2239–2251.

Livingston, J. M., Kapustin, V. N., Schmid, B., Russell, P. B., Quinn, P. K., Bates, T. S., Durkee, P. A. and Freudenthaler, V. 2000. Shipboard sunphotometer measurements of aerosol optical depth spectra and columnar water vapor during ACE-2. *Tellus* **52B**, 594–619.

Mishchenko, M. I., Travis, L. D., Kahn, R. A. and West, R. A. 1997. Modeling phase functions for dustlike tropospheric aerosols using a shape mixture of randomly oriented polydisperse spheroids. *J. Geophys. Res.* **102**, 16831–16847.

Neusüß, C., Weise, D., Birmili, W., Wiedensohler, A. and Covert, D. 2000. Size-segregated chemical, gravimetric and number distribution derived mass closure of the aerosol in Sagres, Portugal during ACE-2. *Tellus* **52B**, 169–184.

Novakov, T., Bates, T. S. and Quinn, P. K. 2000. Shipboard measurements of the concentration and properties of carbon aerosols during ACE-2. *Tellus* **52B**, 228–238.

Novakov, T., Hegg, D. A. and Hobbs, P. V. 1997. Airborne measurements of carbonaceous aerosols on the east coast of the United States, *J. Geophys. Res.* **102**, 30,023–30,030.

Öström, E. and Noone, K. J. 2000. Vertical profiles of aerosol scattering and absorption measured in situ during the North Atlantic Aerosol Characterization Experiment ACE-2. *Tellus* **52B**, 526–545.

Philippin, S., Neusüß, C., Wiedensohler, A., Heintzenberg, J., Carrico, C. M. and Rood, M. J. 1998. Optical

properties of anthropogenically influenced aerosols in a marine atmosphere: an optical closure experiment. *J. Aer. Sci.* **29**, S1151–S1152.

Powell, D. M., Reagan, J. A., Rubio, M. A., Erxleben, W. H. and Spinhirne. J. D. 2000. ACE-2 multiple angle micro-pulse lidar observations from Las Galletas, Tenerife, Canary Islands. *Tellus* **52B**, 652–661.

Putaud, J. P., Van Dingenen, R., Mangoni, M., Virkkula, A., Raes, F. Maring, H., Prospero, J. M., Swietlicki, E., Berg, O. H., Hillamo, R. and Makela, T. 2000. Chemical mass closure and origin assessment of the submicron aerosol in the marine boundary layer and the free troposphere at Tenerife during ACE-2. *Tellus* **52B**, 141–168.

Quinn, P., Coffman, D. J., Bates, T. S. and Covert, D. S. 2000. Chemical and optical properties of ACE-2 aerosol. *Tellus* **52B**, 239–257.

Quinn, P. K., Anderson, T. L., Bates, T. S., Dlugi, R., Heintzenberg, J., Hoyningen-Huene Von, W., Kulmala, M., Russell, P. B. and Swietlicki, E. 1996. Closure in tropospheric aerosol-climate research: a review and future needs for addressing aerosol direct shortwave radiative forcing. *Contr. Atmos. Phys.* **69**, 547–577.

Raes, F., Bates, T., Mcgovern, F. and Van Liedekerke, M., 2000. The Second Aerosol Characterization Experiment (ACE-2): general overview and main results. *Tellus* **52B**, 111–126.

Remer, L. A., Gassó, S., Hegg, D. A., Kaufman, Y. J. and Holben, B. N. 1997. Urban/industrial aerosol: ground-based sun/sky radiometer and airborne in situ measurements. *J. Geophys. Res.* **102**, 16,849–16,859.

Russell, P. B., Kinne, S. and Bergstrom, R. 1997. Aerosol climate effects: local radiative forcing and column closure experiments. *J. Geophys. Res.* **102**, 9397–9407.

Saxena, P., Hildemann, L. M., McMurry, P. H. and Seinfeld, J. H. 1995. Organics alter hygroscopic behavior of atmospheric particles. *J. Geophys. Res.* **100**, 18,755–18,770.

Schmeling, M., Russell, L. M., Erlick, C., Collins, D., Flagan, R. C., Seinfeld, J. H., Jonsson, H., Wang, Q., Kregsamer, P. and Streli, C. 2000. Aerosol particle chemical characteristics measured from aircraft in the lower troposphere during ACE-2. *Tellus* **52B**, 185–200.

Schmid, B., Livingston, J. M., Russell, P. B., Durkee, P. A., Collins, D. R., Flagan, R. C., Seinfeld, J. H., Gassó, S., Hegg, D. A., Öström, E., Noone, K. J., Welton, E. J., Voss, K., Gordon, H. R., Formenti, P. and Andreae, M. O. 2000. Clear sky closure studies of lower tropospheric aerosol and water vapor during ACE-2 using airborne sunphotometer, airborne

in-situ, space-borne, and ground-based measurements. *Tellus* **52B**, 568–593.

Smirnov, A., Holben, B. N., Slutsker, I., Welton, E. J. and Formenti, P. 1998. Optical properties of Saharan dust during ACE-2. *J. Geophys. Res.* **103D**, 28,079–28,092.

Swietlicki, E., Zhou, J., Berg, O. H., Hameri, K., Vakeva, M., Makela, J., Covert, D. S., Dusek, U., Busch, B., Wiedensohler, A. and Stratmann, F. 2000. Hygroscopic properties of aerosol particles in the eastern Northern Atlantic during ACE-2. *Tellus* **B**, this issue.

Tang, I. N., Tridico, A. C. and Fung, K. H. 1997. Thermodynamic and optical properties of sea salt aerosols. *J. Geophys. Res.* **102**, 23,269–23,275.

Tomasi, C., Marani, S., Vitale, V., Wagner, F., Cacciari, A. and Lupi, A. 2000. Precipitable water evaluations from infrared sun-photometric measurements analysed using the atmospheric hygrometry technique. *Tellus* **52B**, 734–749.

Verver G., Raes, F., Vogelezang, D. and Johnson, D. 2000. The second Aerosol Characterization Experiment (ACE-2): meteorological and chemical context, *Tellus* **52B**, 126–140.

Vitale, V., Tomasi, C., Von Hoyningen-Huene, W., Bonafe', U., Marani, S., Lupi, A., Cacciari, A. and Ruggeri, P. 2000. Spectral measurements of aerosol particle extinction in the 0.4–3.7 μm wavelength range, performed at Sagres with the IR-RAD sun-radiometer. *Tellus* **52B**, 716–733.

Von Hoyningen-Huene, W., Schmidt, T., Herber, A. and Silva, A. M. 1998. Climate-relevant columnar optical aerosol parameters obtained during ACE-2 CLEARCOLUMN and their influence on the shortwave radiative balance. *J. Aerosol Sci.* **29**, S269–S270.

Von Hoyningen-Huene, W., Schmidt, T., Freitag, M., Burrows, P. and Silva, A. M. 1999. Closures between ground-based and spaceborne data for the development of retrieval procedures for aerosols properties. *J. Aerosol Sci.* **30**, S431–S432.

Wagner, F., Müller, D., Ansmann, A., Weise, D. and Althausen, D. 1998. *Comparison of aerosol properties derived from lidar, sun photometer and in situ observations during the aerosol characterization experiment 2.* 19th International Laser radar Conference. Annapolis, NASA/CP-1998-207671/PT1, pp. 457–460.

Welton, E. J., Voss, K. J., Gordon, H. R., H. Maring, Smirnov, A., Holben, B., Schmid, B., Livingston, J. M., Russell, P. B., Durkee, P. A., Formenti, P. and Andreae, M. O. 2000. Ground-based lidar measurements of aerosols during ACE-2: instrument description, results, and comparisons with other ground-based and airborne measurements. *Tellus* **52B**, 636–651.